

# Quark Stars as Hideouts For Color-spin-locked Quark Matter: Implications for Powering High-energy Electromagnetic Emissions

Xin-Ying Song <sup>1,2,\*</sup>

<sup>1</sup>University of Chinese Academy of Sciences, Chinese Academy of Sciences, Beijing 100049, China

<sup>2</sup>Key Laboratory of Particle Astrophysics, Institute of high-energy Physics, Chinese Academy of Sciences, Beijing 100049, China

(Dated: October 29, 2024)

The ground state of moderately dense cold quark matter is investigated within the framework of the Nambu-Jona-Lasinio model. It is found that in the regime of weak and intermediate diquark coupling strength, the color-spin-locked (CSL) phase could be most favored, and the density range where CSL phase survives is determined by two quark chemical potentials: one corresponding to the chiral phase transition and the other for the emergence of the gapless color-flavor-locked (CFL) condensate. Based on the theoretical hypothesis that the quark star could be the hideout for CSL quark matter, an interesting scenario is proposed that the phase transition to the CSL phase could occur in the cooling process of a proper quark star. The CSL quark matter is an electromagnetic superconductor of Type-I, and a complete Meissner effect is expected. However, the analysis for this sizable superconductor indicates that most of the magnetic field is frozen inside the star with a critical strength, while in some special cases, a small fraction could be expelled from a thin layer near the surface in a short time. An analysis on energetics and time scale is performed to investigate if this expulsion of magnetic flux could power or induce high-energy electromagnetic emissions.

## I. INTRODUCTION

It is most possible that the quark matter (QM) exists in the core of compact stars, as quarks are deconfined in extremely dense baryon matter, and the strange quark matter is predicted to be the ground state of QCD at finite baryon number [1–5]. In sufficiently cold and dense quark matter, an attractive interaction provided by the gluon exchange, no matter how weak, results in the formation of a quark Cooper pair condensate [6, 7]. This phenomenon is color superconductivity, which is similar to the electronic superconductivity caused by the attractive interaction between electrons mediated by the exchange of virtual phonons in certain metals and alloys (i.e. BCS theory [8]).

The quark pairing in terms of representations of the color gauge group is formulated as the color gauge group  $SU(3)_c$ , i.e.  $[3]_c \otimes [3]_c = [\bar{3}]_c^A \oplus [6]_c^S$ , where the number of colors is three,  $N_c = 3$ . The quarks interact in an antisymmetric ( $A$ ) anti-triplet channel ( $[\bar{3}]_c^A$ ) and a symmetric ( $S$ ) sextet channel ( $[6]_c^S$ ) which are attractive and repulsive, respectively. The spin-zero condensate requires an antisymmetric anti-triplet channel in the flavour ( $f$ ) structure ( $[\bar{3}]_f^A$ ), since the overall wave function of the Cooper pair has to be antisymmetric, which leads to even-parity, spin-singlet pairing. In cold and very dense three-flavour quark matter, the color-flavor locked (CFL) phase is the ground state [7, 9–11]. As the density drops below some critical value of the strange quark mass, it is replaced by the gapless CFL (gCFL) phase [12, 13].

However, as the density continues to decrease, the quark chemical potential ( $\mu$ )<sup>1</sup> is not sufficient to populate any strange quarks, the quark matter should be two-flavor. Thus, some two-flavor condensates are proposed, such the standard two-flavor color-superconducting (2SC) phase, the gapless

2SC (g2SC) phase, as well as unpaired normal quark (NQ) phase. Some theoretical investigations [14–16] have been performed with self-consistent treatment of quark masses to gain the information at moderate chemical potentials. One of the conclusions is that the pure 2SC condensate does not occur for weak and intermediate diquark coupling at low temperatures (less than 10 MeV) while the NQ phase (or the mixed phase of 2SC and NQ) is most favored [16].

In both CFL and 2SC phases the Fermi momenta of the quark flavors participating in pairing are assumed to be equal. This is a necessary condition for the conventional BCS pairing mechanism. However, for moderate densities ( $\mu \sim 400$  MeV), this assumption could be not valid; therefore, the ground state is neither the (pure) CFL nor the (pure) 2SC state [17]. Some other possibilities have been proposed, such as Larkin-Ovchinnikov-Fulde-Ferrell (LOFF) phase [18, 19] and single-flavor pairing. The spin-one state corresponds to the spin-triplet ( $[3]_f^S$ ), thus, the flavor structure ( $[6]_f^S$ ) of color-spin-locked (CSL) phase allows pairing in single-flavor<sup>2</sup>. The gap parameters ( $\Delta$ ) of CSL phase have an order of 10 keV to 1 MeV, which are small compared with those from 2SC and CFL [17].

The electromagnetic (EM) Meissner effect is a matter of debate for the color superconductor (CSC) [20, 21]. There is almost not EM Meissner effect in spin-zero CSC as concluded in some works (e.g., see [20]). In contrast, the CSL condensate is a Type-I EM superconductor and the magnetic field would be expelled from macroscopic regions if it does not exceed the critical magnetic field ( $B_c$ ) [21]. If a quark star (QS) could be a hideout for QM in CSL phase, once the temperature falls below the critical value ( $T_c$ ), the phase transition to the CSL state would affect the properties of the compact star and may lead to observable consequences. It is interesting to

\* songxy@ihep.ac.cn

<sup>1</sup>  $\mu$  is related to the baryon chemical potential by  $\mu_B = 3\mu$ .

<sup>2</sup> In this paper, other spin-one phases (e.g., the polar, A and planar phases) are not considered.

investigate if it could power high-energy EM emissions, such as fast-radio bursts (FRBs), a magnetar giant flares (MGF) of soft gamma-ray repeaters (SGR), and gamma-ray bursts (GRBs).

The paper is organized as follows: in Section II, the models and methods to describe properties of color superconducting phases are introduced briefly; the thermodynamic potential density as a function of  $\mu$  for each phase is numerically determined; in Section III, a static configuration of CSL QS is constructed; the expulsion of magnetic flux induced by the forming of CSL condensate is described; the possible observable consequences are discussed and summarized in Section IV.

## II. THE MODEL FOR QUARK MATTER

The locally neutral three-flavor quark matter is studied within the framework of Nambu–Jona-Lasinio (NJL) model [14, 22, 23]. Constituent quark masses are dynamically generated and treated self-consistently. The mean-field Lagrangian density for quarks is given by

$$\mathcal{L}^{\text{MF}} = \mathcal{L}_0 + \mathcal{L}_{\text{int}}, \quad (1)$$

where the  $\mathcal{L}_0 = \bar{\psi}(i\partial - \hat{m})\psi$  is the free part and quark spinor field  $\psi_f^c$  carries color ( $c = r, g, b$ ) and flavor ( $f = u, d, s$ ) indices; the matrix of quark current masses is given by  $\hat{m} = \text{diag}_f(m_u, m_d, m_s)$ .  $\mathcal{L}_{\text{int}} = \mathcal{L}_{q\bar{q}} + \mathcal{L}_{qq} + \mathcal{L}'_{\text{t hooft}}$ , is the interaction part which includes the quark-antiquark ( $q\bar{q}$ ), diquark ( $qq$ ) and 't Hooft interaction terms. The  $q\bar{q}$  term is given by,

$$\mathcal{L}_{q\bar{q}} = G_S \sum_{a=0}^8 (\bar{\psi}\lambda_a\psi)^2 + (\bar{\psi}i\gamma_5\lambda_a\psi)^2, \quad (2)$$

while the 't Hooft interaction term is given by,

$$\mathcal{L}'_{\text{t hooft}} = -K \left\{ \det_f [\bar{\psi}(1 + \gamma_5)\psi] + \det_f [\bar{\psi}(1 - \gamma_5)\psi] \right\}, \quad (3)$$

where  $G_S$  and  $K$  are constants for  $q\bar{q}$  coupling and 't Hooft interaction respectively.  $\lambda_a$  with  $a = 1, \dots, 8$  are the Gell-Mann matrices in flavor space, and  $\lambda_0 \equiv \sqrt{2/3} \mathbb{1}_f$ . For  $\mathcal{L}_{qq}$ , the spin-0 condensates have different diquark pairing channels from those of spin-1 condensates. For spin-0 cases (the Greek indices signify flavors and the Latin indices signify colors, the same below):

$$\mathcal{L}_{qq, \text{spin}=0} = G_D \sum_{\gamma, c} \left[ \bar{\psi}_\alpha^a i\gamma_5 \epsilon^{\alpha\beta\gamma} \epsilon_{abc} (\psi_C)_\beta^b \right] \left[ (\bar{\psi}_C)_\rho^r i\gamma_5 \epsilon^{\rho\sigma\gamma} \epsilon_{rsc} \psi_\sigma^s \right], \quad (4)$$

where the  $G_D$  is diquark coupling ( $G_D = \frac{3}{4}G_S$  denotes an intermediate diquark coupling strength, while  $G_D = G_S$  denotes a strong one); the charge conjugate spinors are defined as follows:  $\psi_C = C\bar{\psi}^T$  and  $\bar{\psi}_C = \psi^T C$ , where  $\bar{\psi} = \psi^\dagger \gamma^0$  is the Dirac conjugate spinor and  $C = i\gamma^2 \gamma^0$  is the charge conjugation matrix. For the CSL case:

$$\mathcal{L}_{qq, \text{CSL}} = H \sum_{f=u, d, s} [\bar{\psi}_f i\gamma_\nu \lambda_A \psi_C] [\bar{\psi}_{C, f} i\gamma_\nu \lambda_A \psi_f], \quad (5)$$

where  $H = \frac{3}{8}G_S$ ;  $(\nu, A) = (3, 2), (1, 7)$  and  $(2, 5)$ .

The grand partition function, up to an irrelevant normalization constant, is given by

$$\mathcal{Z} \equiv e^{-\Omega V/T} = \int \mathcal{D}\bar{\psi} \mathcal{D}\psi e^{i \int_X (\mathcal{L} + \bar{\psi} \hat{\mu} \gamma^0 \psi)}, \quad (6)$$

where  $\Omega$  is the thermodynamic potential density,  $V$  is the volume of the three-space, and  $\hat{\mu}$  is a diagonal matrix of quark chemical potentials which will be specified in different cases,  $\mu_{ab}^{\alpha\beta} = \left( \mu \delta^{\alpha\beta} + \mu_Q Q_f^{\alpha\beta} \right) \delta_{ab} + [\mu_3 (T_3)_{ab} + \mu_8 (T_8)_{ab}] \delta^{\alpha\beta}$ . In chemical equilibrium, the nontrivial components of this matrix are extracted from the following relation:  $\mu_Q$  is the chemical potential of electric charge (in the following,  $\mu_e = -\mu_Q$ ), while  $\mu_3$  and  $\mu_8$  are color chemical potentials associated with two mutually commuting color charges of the  $SU(3)_c$  gauge group. The explicit form of the electric charge matrix is  $Q_f = \text{diag}_f(\frac{2}{3}, -\frac{1}{3}, -\frac{1}{3})$ , and the explicit form of the color charge matrices are  $T_3 = \text{diag}_c(\frac{1}{2}, -\frac{1}{2}, 0)$  and  $\sqrt{3}T_8 = \text{diag}_c(\frac{1}{2}, \frac{1}{2}, -1)$ .

The interaction terms are linearized in the presence of the diquark condensates ( $\Delta_{c, \text{spin}=0} \propto (\bar{\psi}_C)_\alpha^a i\gamma_5 \epsilon^{\alpha\beta c} \epsilon_{abc} \psi_\beta^b$  for spin-0 cases and  $\Delta_{f, \text{CSL}} \propto \bar{\psi}_f i\gamma_\nu \lambda_A \psi_C$  for the CSL state) and quark-antiquark condensates ( $\sigma_\alpha \sim \bar{\psi}_\alpha^a \psi_\alpha^a$ ). The thermal potential for the case of spin-0 is given by<sup>3</sup>,

$$\begin{aligned} \Omega_{\text{spin}=0} &= \Omega_e - \Omega_{\text{vac}} + \frac{1}{4G_D} \sum_{i=1}^3 |\Delta_i|^2 + 2G_S \sum_{\alpha=1}^3 \sigma_\alpha^2 \\ &\quad - 4K \sigma_u \sigma_d \sigma_s - T \sum_n \int_{|\mathbf{k}| < \Lambda} \frac{d^3 k}{(2\pi)^3} \frac{1}{2} \text{Tr} \ln \frac{S^{-1}(i\omega_n, \mathbf{k})}{T}, \end{aligned} \quad (7)$$

while that for CSL phase is,

$$\begin{aligned} \Omega_{\text{CSL}} &= \Omega_e - \Omega_{\text{vac}} + \frac{1}{H} \sum_{f=u, d, s} |\Delta_f|^2 + 2G_S \sum_{\alpha=1}^3 \sigma_\alpha^2 \\ &\quad - 4K \sigma_u \sigma_d \sigma_s - T \sum_n \int_{|\mathbf{k}| < \Lambda} \frac{d^3 k}{(2\pi)^3} \frac{1}{2} \text{Tr} \ln \frac{S_f^{-1}(i\omega_n, \mathbf{k})}{T}, \end{aligned} \quad (8)$$

where  $\Omega_e$  is the thermodynamic potential of ultrarelativistic electrons.  $\Omega_{\text{vac}}$  is contribution from the vacuum at  $T = \mu = 0$ , i.e. the bag constant; it is the thermodynamic potential of nontrivial vacuum which is dynamically generated in NJL model, and has been subtracted in order to get zero pressure in vacuum. In real QCD the ultraviolet modes decouple because of asymptotic freedom, but in the NJL model this feature is added by hand, through a UV momentum cutoff  $\Lambda$  in the momentum integrals. In Equation (7),  $S^{-1}$  is the inverse full

<sup>3</sup> Two general formulae are used in the derivation:  $\int d^D x e^{-\frac{1}{2} x \hat{A} x} = (2\pi)^{\frac{D}{2}} (\det \hat{A})^{-\frac{1}{2}}; \ln \det |\hat{A}| = \text{Tr}(\ln \hat{A})$  (see [24]).

quark propagator in the Nambu-Gorkov representation,

$$S^{-1} = \begin{pmatrix} [G_0^+]^{-1} & \Phi^- \\ \Phi^+ & [G_0^-]^{-1} \end{pmatrix}, \quad (9)$$

with the diagonal elements being the inverse Dirac propagators of quarks and of charge-conjugate quarks,

$$[G_0^\pm]^{-1} = \gamma^\nu k_\nu \pm \hat{\mu}\gamma_0 - \hat{M}, \quad (10)$$

where  $k^\mu = (k_0, \mathbf{k})$  denotes the four-momentum of the quark.  $\hat{M} = \text{diag}_f(M_u, M_d, M_s)$  is the constituent mass matrix, and defined as,

$$M_\alpha = m_\alpha - 4G_S\sigma_\alpha + 2K\sigma_\beta\sigma_\gamma, \quad (11)$$

which is treated self-consistently as dynamically generated quantity. The definition of  $S_f^{-1}$  in Equation (8) and corresponding derivation are similar. The details of evaluations for  $\Omega_{\text{spin}=0}$  and  $\Omega_{\text{CSL}}$  are presented in Appendix A. The set of parameters are listed as below [25],

$$m_{u,d} = 5.5 \text{ MeV}, \quad (12a)$$

$$m_s = 140.7 \text{ MeV}, \quad (12b)$$

$$G_S\Lambda^2 = 1.835, \quad (12c)$$

$$K\Lambda^5 = 12.36, \quad (12d)$$

$$\Lambda = 602.3 \text{ MeV}, \quad (12e)$$

which could reproduce the masses of mesons of vacuum QCD. The constituent masses in vacuum for light and strange quarks are 368 MeV and 549 MeV, which are the stable solution for  $\Omega_{\text{vac}}$ , as shown in FIG. 1 (a).

The gaps and dynamic quark masses are determined by minimization of the grand canonical thermodynamical potential as

$$\frac{\partial\Omega}{\partial\sigma_\alpha} = 0, \quad (13a)$$

$$\frac{\partial\Omega}{\partial\Delta_{i(f)}} = 0. \quad (13b)$$

Since the quark matter should be locally color and electric charge neutral, the color and electric chemical potentials are evaluated by enforcing zero color and electric charge as,

$$n_e \equiv -\frac{\partial\Omega}{\partial\mu_e} = 0, \quad (14a)$$

$$n_3 \equiv -\frac{\partial\Omega}{\partial\mu_3} = 0, \quad (14b)$$

$$n_8 \equiv -\frac{\partial\Omega}{\partial\mu_8} = 0. \quad (14c)$$

Note that the CSL phase is naturally color neutral, thus it is not necessary to impose color neutrality and one has  $\mu_3 = \mu_8 = 0$ . The calculation is performed at  $T = 0$  to approximately obtain the properties of QM in a cold QS. According to the conclusion of previous work [16], in the regime of weak and intermediate diquark coupling strength, the unpaired normal quark (NQ) phase is most favored in the moderately dense

matter at  $T \lesssim 10$  MeV, however, color-superconducting condensates considered in that work are only those of spin-0. The CSL phase could be more favored than the NQ phase at some densities [26]. Therefore, we should compare these minima of thermodynamical potential to find the most stable phase at different densities. The types and gaps of phases are listed as below,

- 2SC:  $\Delta_3 > 0, \Delta_2 = \Delta_1 = 0$ ; the gaps  $\Delta_1, \Delta_2$ , and  $\Delta_3$  correspond to the down-strange, the up-strange and the up-down diquark condensates, respectively;
- CSL: each flavor is paired, and the gap is  $\Delta_f$ ;
- NQ:  $\Delta_3 = \Delta_2 = \Delta_1 = 0$ ;
- (g)CFL:  $\Delta_3 \gtrsim \Delta_2 = \Delta_1$ ; as  $\mu$  decreases, one has CFL  $\rightarrow$  gCFL, and  $\Delta_3 > \Delta_2 > \Delta_1 > 0$ .

The dynamical quark masses and gaps of CSL condensate in the moderate chemical potentials are shown in FIG. 1 (a). When  $\mu \geq 368$  MeV, the light quarks are populated, and strange quark mass in vacuum falls from 549 MeV to about 464 MeV due to the flavor mixing [14]. The gaps  $\Delta_{u,d}$  range from hundreds of keV to a few MeV. Above  $\mu = 433$  MeV (denoted by a cyan star as shown in FIG. 1 (a)), the value of  $\mu + \mu_e/3$  begins to be larger than  $M_s$  in vacuum, and the density of strange quarks becomes nonzero.

Minima of the thermodynamical potential for QM at  $T = 0$  as a function of  $\mu$  are shown in FIG. 1 (b). For  $G_D/G_S = 3/4$ , gCFL is most favored at 443 MeV  $\lesssim \mu \lesssim 457$  MeV, which is denoted by a narrow blue shadow<sup>4</sup>. Although the difference between the  $\Omega_{\text{min}}^{\text{CSL}}$  and  $\Omega_{\text{min}}^{\text{NQ}}$  is small as shown in the sub-plot in FIG. 1 (b), the CSL phase is more stable than that of NQ at moderate densities. Therefore, the most favored phase for 368 MeV  $< \mu < 443$  MeV is CSL. Note that for  $\mu \gtrsim 445$  MeV ( $\mu = 445$  MeV at which  $\Omega_{\text{min}}^{2\text{SC}} = \Omega_{\text{min}}^{\text{NQ}}$  is denoted by a dotted vertical line), the 2SC phase begins to be more stable than the NQ phase, which is consistent with the result of [16]. For  $G_D/G_S = 1$ , 2SC is the most favored phase at the moderate chemical potentials, however, this is not the case that interests us.

In this section, the density range where the CSL phase survives is determined as 368 MeV  $\leq \mu \leq 443$  MeV at zero temperature for the intermediate diquark coupling by two critical quark chemical potentials: one corresponding to the chiral phase transition from the nontrivial vacuum to the deconfined light quarks and the other for the emergence of the gCFL condensate.

### III. THE CSL QUARK STAR CONFIGURATION AND EXPULSION OF MAGNETIC FLUX

The QS as a hideout for quark matter in CSL phase could have two configurations. One has pure CSL QM, thus the

<sup>4</sup> The calculation for gCFL is not performed in this paper; numerical results of gCFL from [16] are used in the FIG. 1 (b).

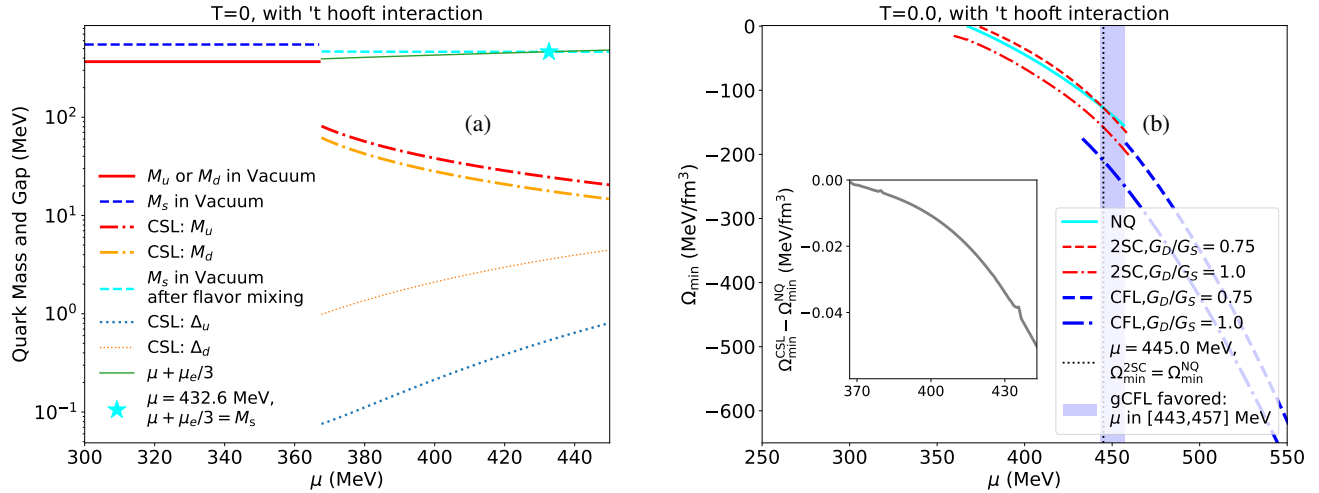


FIG. 1. (a) The dynamic quark masses and gaps in CSL phase. The blue dashed line denotes  $M_{s, \text{Vac}} = 549$  MeV in vacuum, while the cyan dashed line denotes  $M_{s, \text{Vac}}$  around 464 MeV in vacuum due to the flavor mixing with considering 't hooft interaction. The dot-dashed lines denote the dynamic masses of light quarks, while the dotted lines denote the gaps. The green thin solid line denotes the values of  $\mu_s = \mu + \mu_e/3$  varying with  $\mu$ , with a cyan star denoting the point of  $\mu_s = M_s$ . (b) Minima of the thermodynamical potential for neutral three-flavor quark matter at  $T = 0$  as a function of the quark chemical potential. The red dashed and dot-dashed lines denote  $\Omega_{\min}$  in 2SC phase with  $G_D/G_S = 0.75$  and  $G_D/G_S = 1.0$ , while the blue ones denote those of CFL phases. The solid cyan line denotes  $\Omega_{\min, NQ}$ . The blue shadow denotes the region that the gCFL phase is most favored. The dotted vertical line ( $\mu = 445$  MeV) denotes the beginning that the 2SC phase becomes more stable than NQ and CSL phases.

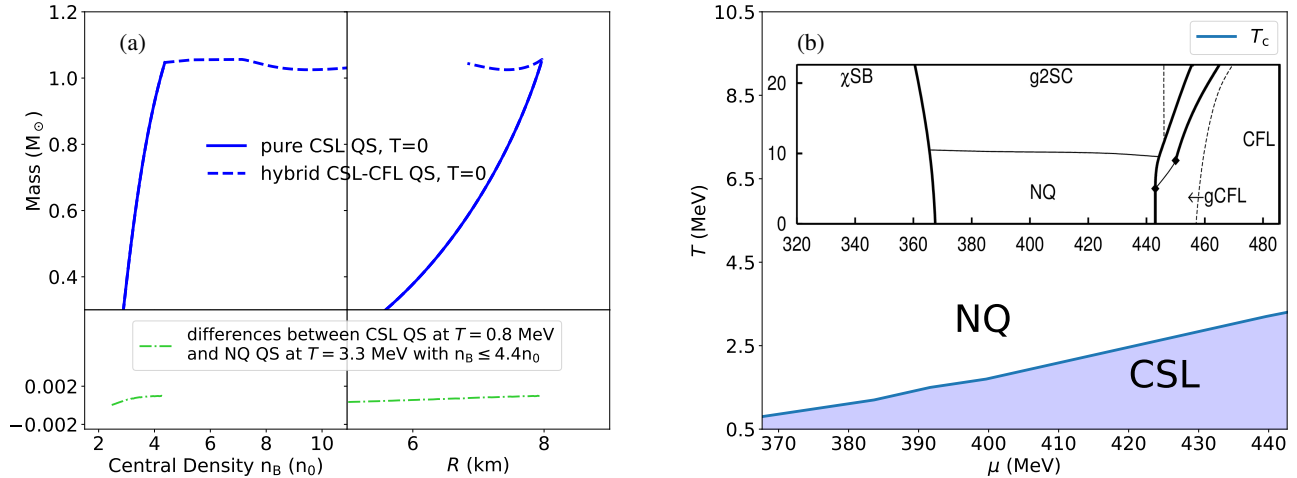


FIG. 2. (a) Sequences of cold quark stars for the quark matter equation of state in CSL (solid blue lines) and hybrid CSL-CFL (dashed blue lines) phases. The upper left panel shows the rising branches in the  $M-n_B$  relation, while the upper right panel shows the  $M-R$  relation. The lower panels show the differences between CSL QS at  $T = 0.8$  MeV and NQ QS at  $T = 3.3$  MeV on  $M-n_B$  and  $M-R$  relations. (b)  $T - \mu$  phase diagram. The blue line denotes  $T_c$  with respect to  $\mu$ , while the blue shadow denotes the region where CSL phase is favored. The sub-plot is adapted from Figure 1 in [16], which shows the  $T - \mu$  phase diagram of NQ and spin-zero condensates at  $T \lesssim 20$  MeV and  $\mu \lesssim 480$  MeV. The region where the approximate chiral symmetry is broken because of the large constituent quark masses in vacuum is labeled with  $\chi$ SB. The gapless 2SC (g2SC) phase is favored above 10 MeV at moderate densities. Some other favored phases at  $T > 5$  MeV and  $\mu > 443$  MeV have no relationship with the topic discussed in the paper, thus they are not labeled.

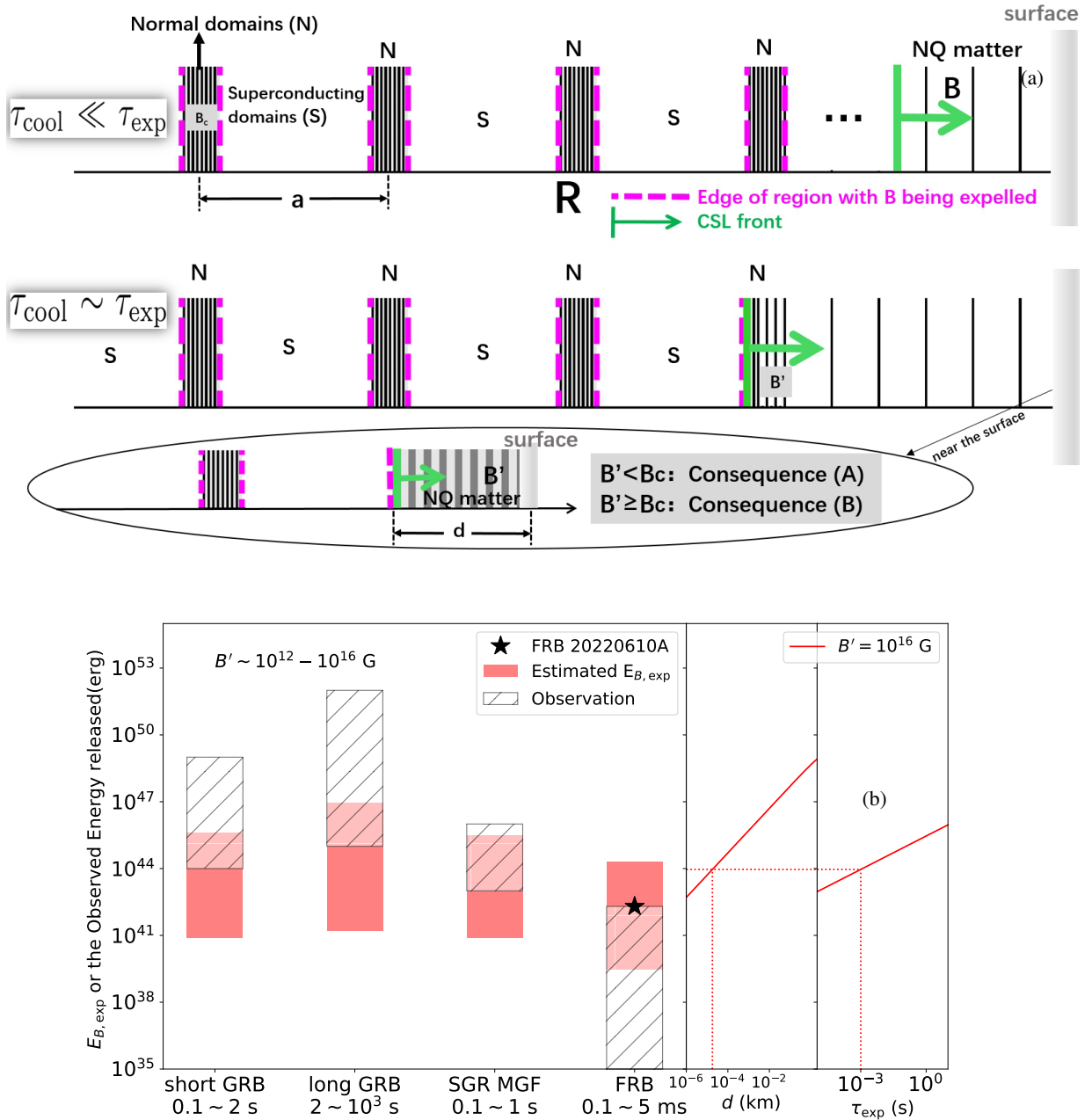


FIG. 3. (a) The sketch for the process of the expulsion of magnetic flux in the cases of  $\tau_{cool} \ll \tau_{exp}$  (the first row) and  $\tau_{cool} \sim \tau_{exp}$  (the second row with a elliptical sub-plot). The green thick vertical lines with arrows denote the CSL fronts. The pink dashed lines denote the edges of regions with  $B$  being expelled. The regions filled with sparse vertical solid lines denotes the NQ matter with magnetic field  $B$ . The blank regions labeled with ‘S’ denote the superconducting domains, while those regions labeled with ‘N’ and filled with dense vertical lines between two dashed lines denote normal regions with critical magnetic field  $B_c$  (densities of these lines do not represent the strength of magnetic field precisely, but for identification purpose only). The detailed description about the process is in the text, and the dimensions in this figure are distorted for clarity. (b) The comparison between the estimated  $E_{B,exp}$  in the hypothesis of Consequence (A) and observations from different high-energy emissions.

central density ( $n_B$ ) should be not be larger than  $4.4n_0$  (corresponds to the critical chemical potential  $\mu_{CSL \rightarrow gCFL} = 443$  MeV), where  $n_0 = 0.16 \text{ fm}^{-3}$  is the nuclear saturation density. The other one has a core in CFL phase with  $n_B > 4.4n_0$ .

Besides, it is necessary to investigate the density range

where the neutron star matter is more stable than CSL QM. A similar calculation performed in NJL model indicates that thermodynamical potential of QM is lower than that of neutron star matter starting from  $\mu_B \sim 1.1$  GeV (corresponding

to  $\mu \sim 367$  MeV [27]<sup>5</sup>. Therefore, the existence of pure CSL QS is possible within the framework of NJL model.

A spherically symmetric, static configuration of dense matter can be determined with the well-known Tolman-Oppenheimer-Volkoff (TOV) equation for hydrostatic equilibrium of self-gravitating matter [28],

$$\frac{dP(r)}{dr} = -\frac{[\varepsilon(r) + P(r)][m(r) + 4\pi r^3 P(r)]}{r[r - 2m(r)]}. \quad (15)$$

Here  $\varepsilon(r)$  is the energy density and  $P(r)$  the pressure at distance  $r$  from the center of the star. The mass enclosed in a sphere with radius  $r$  is defined by

$$m(r) = 4\pi \int_0^r \varepsilon(r') r'^2 dr'. \quad (16)$$

The mass-radius ( $M$ - $R$ ) relationships of static CSL QS and hybrid CSL-CFL QS are shown in FIG. 2 (a), which are obtained by solving Equations (15) and (16) for given  $n_B$ . The maximum QS mass for a non-rotating QS could reach up to  $1.06 M_\odot$ , with a radius of about 8 km. With increasing density, a phase transition to the (g)CFL phase renders the sequence unstable. The QS could have a nuclear crust when surface boundary conditions are properly taken into account, however, the volume of CSL QM inside must be less than that of a bare CSL QS. Moreover, a hybrid star with a CFL core can not have a larger volume of CSL QM for the same reason in the static state.

The magnetic field ( $B$ ) energy inside the QS could be estimated as,

$$E_B = \frac{B^2}{8\pi} \left( \frac{4\pi}{3} R^3 \right) \quad (17)$$

$$= 1.7 \times 10^{47} \text{erg} \left( \frac{B}{10^{15} \text{G}} \right)^2 \left( \frac{R}{10 \text{km}} \right)^3. \quad (18)$$

Let us assume a QS with  $n_B \lesssim 4.4n_0$  and initial temperature of about 10 MeV in the cooling process. When the temperature falls below 10 MeV, the NQ phase becomes the most stable phase as shown in the sub-plot in FIG. 2 (b); the magnetic field can penetrate the NQ matter, and for simplicity, we assume  $B$  inside the star is uniform. The larger densities correspond to larger  $T_c$  as shown in FIG. 2 (b). Considering the relation between the density and  $r$ ,  $T_c = 3.3$  MeV at  $\mu = 443$  MeV in the core ( $r = 0$ ) of the QS, while  $T_c$  decreases to about 0.8 MeV at  $\mu = 368$  MeV near the surface ( $r = R$ ). During the cooling process from  $T = 3.3$  MeV to 0.8 MeV, the phase transition occurs from NQ to CSL state; changes on the equation of state could be ignored due to the small gaps of CSL condensate, as indicated by the differences on  $M$ - $R$  and  $M$ - $n_B$  relationships shown in the lower panels in FIG. 2 (a).

Since the QS core has the largest  $T_c$ , one may expect that the CSL condensate forms first in the central of the star dur-

ing the cooling process<sup>6</sup>. In a simplified picture, the CSL condensate forms along the edge of NQ matter cooling down to  $T_c$ , thus  $\tau_{\text{cool}}$  could be taken as the time-scale of CSL front expanding. The consequence of expulsion of magnetic flux during the cooling and phase transition process is affected by the competition between the characteristic time-scale ( $\tau_{\text{exp}}$ ) of the expulsion of magnetic flux and  $\tau_{\text{cool}}$ ; it is discussed in different cases as follows.

#### A. The 1st Case: $\tau_{\text{cool}} \ll \tau_{\text{exp}}$

Alternating regions of normal and superconducting matters form during this process as sketched in FIG. 3 (a). This is the so-called intermediate state of the Type-I superconductor with a configuration consisting of a mixture of normal and superconducting domains [29–31]. The expulsion of magnetic flux means that supercurrents form in CSL QM, offset the magnetic field inside to form a superconducting domain and enhance that of outside to keep the total flux a constant.  $B'$  denotes the magnetic field enhanced in the outside of the superconducting domain. The expulsion around the region containing  $B'$  continues until  $B' = B_c$ , and a normal domain forms. As the CSL front expands, similar structures form subsequently behind it on a fine scale as shown in the first row in FIG. 3 (a). The periodicity length  $a$  (distance from center to center between two neighboring normal or superconducting domains) is given by [30]:

$$a = \sqrt{\delta \times D / f(\tilde{B})}, \quad (19)$$

where  $\delta$  denotes the wall-energy parameter, and the wall-energy is associated with the interface separating a normal from a superconducting domain;  $D$  denotes the thickness of the superconductor placed perpendicularly in a magnetic field. In the case of  $\tau_{\text{cool}} \ll \tau_{\text{exp}}$ , the CSL front quickly reaches the surface, thus  $D \sim R$  and has an order of 10 km.  $f(\tilde{B})$  is a numerical function of the reduced field  $\tilde{B} = B/B_c$ ; it reaches the maximum of 0.023 with  $\tilde{B} \simeq 0.5$  (see Fig 2.6 in [31]).  $\delta$  is given by,

$$\delta \equiv \xi - \lambda, \quad (20)$$

where  $\xi$  is the coherence length, which is approximately equal to the inverse of the gap, i.e.  $\xi \sim 1/\Delta$ ; for given  $\Delta \sim 1$  MeV in CSL phase,  $\xi \simeq 200$  fm;  $\lambda$  denotes the penetration depth for the magnetic field in CSL QM and has the order of fm [21], thus one has  $\lambda \ll \xi$  and  $\delta \sim \xi$ . With given  $B \sim B_c/2$  ( $B_c$  has the order of  $10^{16}$  G [21]),  $a$  is estimated to be about  $10^{-7}$  km, which is much smaller than the size of QS. The expulsion of a small fraction of  $E_B$  from the star happens only if the surface is located in some superconducting domain, and

<sup>5</sup> Note that in that work, spin-one condensates are not considered.

<sup>6</sup> The cooling of QS is governed by the general relativistic thermal balance, transport properties of the quark matter and the crust properties, which is very complex and not discussed in this work. However, it does not affect our conclusion.

$a$  could be taken as the thickness of the thin layer containing the expelled  $E_B$ . With Equation (18),  $E_B$  in this thin layer ( $R - a < r < R$ ) is estimated to be smaller than  $10^{42}$  erg for given  $B \sim B_c/2$ , which accounts a small fraction of the total energy inside.

### B. The 2nd Case: $\tau_{\text{cool}} \sim \tau_{\text{exp}}$

In this case, the edge of the region with  $B$  being expelled almost moves together with the CSL front. Note that the region of enhanced  $B'$  forms ahead of CSL front in the NQ matter, as shown in the second row in FIG. 3 (a). Similar alternating structures form once  $B' \geq B_c$  is valid locally<sup>7</sup>. When the CSL front (and the edge of the region with  $B$  being expelled) gradually approaches the surface with a distance  $d$ , there would be two possible consequences as shown in the elliptical sub-plot in the second row of FIG. 3 (a):

- Consequence (A):  $B' < B_c$  is valid during the following process; the magnetic flux containing in the layer in range of  $R - d < r < R$  is expelled from the star (or CSL core);
- Consequence (B):  $B' \geq B_c$ , thus the expulsion stops.

$\tau_{\text{exp}}$  of the expulsion of magnetic flux in NQ matter is estimated as [29, 32],

$$\tau_{\text{exp}} \simeq \frac{4\pi\sigma_{\text{el}}}{c^2} \left(\frac{d}{\pi}\right)^2 \left(\frac{B'}{H_c}\right)^2, \quad (21)$$

where  $\sigma_{\text{el}}$  is the electrical conductivity,  $d$  is the scale of variation of the magnetic field, and  $H_c \sim 10^{19}$  G is the thermodynamical critical field [33]. The electron conductivity  $\sigma_{e,\text{el}}$  is given by the classical expression,

$$\sigma_{e,\text{el}} = \frac{8\pi\alpha_e n_e l_e}{m_e \bar{v}_e}, \quad (22)$$

where the  $\alpha_e = \frac{1}{137}$  is the QED fine structure constant;  $n_e$  is the electron number density;  $l_e$  is the electron mean free path, which could be estimated as  $n_e^{-1/3}$ ;  $m_e$  is the electron mass and  $\bar{v}_e \simeq \sqrt{\frac{T}{m_e}}$  the average thermal velocity of the electrons.  $\sigma_{\text{el}}$  ranges from  $2.2 \times 10^{23} \text{ s}^{-1}$  at  $\mu = 368 \text{ MeV}$  to  $4.2 \times 10^{23} \text{ s}^{-1}$  at  $\mu = 443 \text{ MeV}$  at  $T \sim 1 \text{ MeV}$ . The quark electric conductivity is given by [34],

$$\sigma_{q,\text{el}} = \left(\alpha_s \frac{T}{0.08 \text{ MeV}}\right)^{-5/3} \left(\frac{\mu}{300 \text{ MeV}}\right)^{8/3} \times 10^{19} \text{ s}^{-1}, \quad (23)$$

<sup>7</sup> Note that  $\tau_{\text{cool}} \sim \tau_{\text{exp}}$  and  $B' < B_c$  being valid during the whole process is an extreme case;  $\tau_{\text{exp}}$  for all the magnetic field inside the star is about  $3 \times 10^6 \text{ s}$  for given  $B = 10^{15} \text{ G}$  and  $d = 8 \text{ km}$ . The emission of this long duration, even if it exists, is beyond the scope of high-energy EM emissions discussed in this paper.

where  $\alpha_s$  is the strong coupling constant and we take  $\alpha_s = 1$  at  $T \sim 1 \text{ MeV}$  and  $\mu \sim 400 \text{ MeV}$ .  $\sigma_{q,\text{el}}$  has the order of  $10^{17} \text{ s}^{-1}$ , which is much smaller than  $\sigma_{e,\text{el}}$ . Therefore,  $\sigma_{\text{el}}$  is mainly contributed by electrons in NQ matter.

For Consequence (A), if it is assumed that  $E_{B,\text{exp}}$  could convert to energies of other forms which lead to high-energy EM emissions, the relationship between  $\tau_{\text{exp}}(d)$  and the duration ( $\tau_{\text{dur}}$ ) of the corresponding emission is:

$$\tau_{\text{dur}} = \tau_{\text{exp}}(d) + \tau_{\text{rel}}, \quad (24)$$

where  $\tau_{\text{rel}}$  denotes the possible relaxation time in the production of the emission. Thus, in this hypothesis,  $\tau_{\text{exp}}(d) \lesssim \tau_{\text{dur}}$ , and a loose upper limit of  $E_{B,\text{exp}}$  could be estimated by  $\tau_{\text{dur}}$  (as shown in the first panel of FIG. 3 (b) in red solid bars).

## IV. DISCUSSION AND SUMMARY

Some high-energy EM emissions can be excluded or allowed in the hypothesis of Consequence (A). For GRBs, the typical energy of the relativistic outflow is estimated to be  $f_b E_{\text{iso},\gamma}/\eta_\gamma$ , where  $f_b \simeq \theta^2/2$  of the order of  $10^{-4} - 10^{-3}$  is the beam factor and  $\theta$  is the beam opening angle;  $E_{\text{iso},\gamma}$  is isotropic-equivalent radiated energy, ranging from  $10^{48} - 10^{52}$  erg for short GRBs and  $10^{49} - 10^{55}$  erg for long GRBs;  $\eta_\gamma$  is the radiative efficiency [35]. The total energy of the outflow of GRB has an order of  $10^{44} - 10^{52}$  erg, as shown in hatched bars in FIG. 3 (b). Though there exist overlaps between observations and  $E_{B,\text{exp}}$ , considering  $\eta_\gamma < 1$ , the expulsion of magnetic flux because of the CSL condensate forming discussed in Section III can not provide enough energy for GRBs.

As suggested in [36], strange star heating events could be taken as a model for GF of SGRs, with the surface of QS heated by impacts of falling massive cometlike objects. Similarly, the surface of QS could be heated in Consequence (A) via magnetic reconnection if the expelled magnetic field lines cross with external ones. A similar mechanism [37] has been suggested to generate SGR; the cooled QS has a CFL core acting as a Type-II superconductor in that work and subsequent bursts result from restructuring of the surface magnetic field because of the vortex dynamics. The typical energy of GF is  $10^{43} - 10^{46}$  erg [38], which seems larger compared with  $E_{B,\text{exp}}$  as shown in FIG. 3 (b). Thus, even if GFs could be induced by the phase transition to CSL condensate, energy provided by the external magnetic field is necessary.

In some theoretical works (e.g., see [39, 40]), FRBs have been proposed to originate from starquakes. The expulsion of magnetic flux in a short time could lead to an intense evolution of magnetic fields in the magnetosphere, and triggering starquakes by converting  $E_{B,\text{exp}}$  to kinematic energies of plasma in the magnetosphere and crust [40, 41]. In the hypothesis of Consequence (A), the millisecond-duration corresponds to  $d \sim 10^{-5} \text{ km}$  and an upper limit of  $E_{B,\text{exp}} \sim 10^{44}$  erg if  $B' = 10^{16} \text{ G}$ , which means that the expelled magnetic flux is contributed from a thin layer, as shown in the second and third panel in FIG. 3 (b). Typical FRBs exhibit isotropic radiative energies of  $10^{35} - 10^{42}$  erg with the maximum energy reaching up to  $2 \times 10^{42}$  erg in FRB 20220610A [42],

which are well below the upper limit of  $E_{B,\text{exp}} \sim 10^{44}$  erg as shown in FIG. 3 (b).

In this paper, we investigate the density range of QM where CSL phase is most favored, and construct a static CSL QS with constraints from the NJL model. A possible special scenario is proposed that a small fraction of magnetic field is expelled from a thin layer near the surface of QS during the phase transition to CSL state, while most of  $E_B$  is frozen inside the star. In conclusion, our analysis suggests that the forming of CSL condensate in QS could act as an inducement mechanism in some special cases, to power typical FRBs, but as a single source of energy, it is unlikely to generate other EM emissions such as GRBs and GFs. However, these conclusions are based on the theoretical hypothesis that the QS could be the hideout for CSL QM, and it would be constrained by the macroscopic astrophysical phenomena observed in the future research.

### ACKNOWLEDGMENTS

The author thank supports from the National Program on Key Research and Development Project (2021YFA0718500) and National Natural Science Foundation of China (grant No. 12303052). The author is very grateful to the suggestions and comments from Prof. Shuang-Nan Zhang. I thank Prof. Shuang-shi Fang for polishing the language in some paragraphs. I am very grateful for the comments and suggestions from the anonymous referees.

### Appendix A: Evaluation of the dispersion relations for spin-0 and CSL condensate

At nonzero temperature, the Matsubara imaginary time formalism is used. The energy  $k_0$  is replaced with  $-i\omega_n$  where  $\omega_n \equiv (2n+1)\pi T$  are the fermionic Matsubara frequencies. The determinant of the inverse quark propagator can be decomposed as follows:

$$\det \frac{S^{-1}}{T} = \prod_i \left( \frac{\omega_n^2 + \epsilon_i(\mathbf{k})^2}{T^2} \right)^2. \quad (\text{A1})$$

The Matsubara summation in Equation (7) can then be done analytically by employing the relation,

$$\sum_n \ln \left( \frac{\omega_n^2 + \epsilon_i^2}{T^2} \right) = \frac{|\epsilon_i|}{T} + 2 \ln \left( 1 + e^{-\frac{|\epsilon_i|}{T}} \right). \quad (\text{A2})$$

Thus, we need to calculate the dispersion relations of  $\epsilon_i$  corresponding to zeros of  $\det S^{-1}$ , i.e. the values of the energy at which the propagator diverges,

$$\det S^{-1}(\epsilon_i(\mathbf{k}), \mathbf{k}) = 0. \quad (\text{A3})$$

For the spin-zero case, the off-diagonal components of the propagator (9) are the so-called gap matrices given in terms of

three diquark condensates. The color-flavor structure of these matrices is given by

$$(\Phi^-)_{ab}^{\alpha\beta} = - \sum_c \epsilon^{\alpha\beta c} \epsilon_{abc} \Delta_c \gamma_5, \quad (\text{A4})$$

and  $\Phi^+ = \gamma^0 (\Phi^-)^\dagger \gamma^0$ . Here, as before,  $a$  and  $b$  refer to the color components and  $\alpha$  and  $\beta$  refer to the flavor components. Hence, the gap parameters  $\Delta_1$ ,  $\Delta_2$ , and  $\Delta_3$  correspond to the down-strange, the up-strange and the up-down diquark condensates, respectively. All three of them originate from the color-antitriplet, flavor-antitriplet diquark pairing channel.  $S^{-1}$  is a  $72 \times 72$  (color: 3, flavor: 3, Dirac:  $4 \times 2$ ) matrix. With a proper ordering of its rows and columns, it decomposes into 6 diagonal blocks of dimension  $4 \times 4$  and one diagonal block of dimension  $12 \times 12$ . The explicit form of these blocks reads

$$\mathcal{M}_+^{(1)} = \begin{pmatrix} -\mu_d^r + M_d & k & 0 & -\Delta_3 \\ k & -\mu_d^r - M_d & \Delta_3 & 0 \\ 0 & \Delta_3 & \mu_u^g + M_u & k \\ -\Delta_3 & 0 & k & \mu_u^g - M_u \end{pmatrix}, \quad (\text{A5a})$$

$$\mathcal{M}_+^{(2)} = \begin{pmatrix} \mu_d^r - M_d & k & 0 & -\Delta_3 \\ k & \mu_d^r + M_d & \Delta_3 & 0 \\ 0 & \Delta_3 & -\mu_u^g - M_u & k \\ -\Delta_3 & 0 & k & -\mu_u^g + M_u \end{pmatrix}, \quad (\text{A5b})$$

$$\mathcal{M}_+^{(3)} = \begin{pmatrix} -\mu_s^r + M_s & k & 0 & -\Delta_2 \\ k & -\mu_s^r - M_s & \Delta_2 & 0 \\ 0 & \Delta_2 & \mu_u^b + M_u & k \\ -\Delta_2 & 0 & k & \mu_u^b - M_u \end{pmatrix}, \quad (\text{A5c})$$

$$\mathcal{M}_+^{(4)} = \begin{pmatrix} \mu_s^r - M_s & k & 0 & -\Delta_2 \\ k & \mu_s^r + M_s & \Delta_2 & 0 \\ 0 & \Delta_2 & -\mu_u^b - M_u & k \\ -\Delta_2 & 0 & k & -\mu_u^b + M_u \end{pmatrix}, \quad (\text{A5d})$$

$$\mathcal{M}_+^{(5)} = \begin{pmatrix} -\mu_s^g + M_s & k & 0 & -\Delta_1 \\ k & -\mu_s^g - M_s & \Delta_1 & 0 \\ 0 & \Delta_1 & \mu_d^b + M_d & k \\ -\Delta_1 & 0 & k & \mu_d^b - M_d \end{pmatrix}, \quad (\text{A5e})$$

$$\mathcal{M}_+^{(6)} = \begin{pmatrix} \mu_s^g - M_s & k & 0 & -\Delta_1 \\ k & \mu_s^g + M_s & \Delta_1 & 0 \\ 0 & \Delta_1 & -\mu_d^b - M_d & k \\ -\Delta_1 & 0 & k & -\mu_d^b + M_d \end{pmatrix}, \quad (\text{A5f})$$

and

$$\mathcal{M}_+^{(7)} = \begin{pmatrix} -\mu_u^r - M_u & k & 0 & 0 & 0 & 0 & 0 & -\Delta_3 & 0 & 0 & 0 & 0 & -\Delta_2 \\ k & -\mu_u^r + M_u & 0 & 0 & 0 & 0 & 0 & \Delta_3 & 0 & 0 & 0 & \Delta_2 & 0 \\ 0 & 0 & \mu_u^r - M_u & k & 0 & \Delta_3 & 0 & 0 & 0 & 0 & \Delta_2 & 0 & 0 \\ 0 & 0 & 0 & k & \mu_u^r + M_u & -\Delta_3 & 0 & 0 & 0 & -\Delta_2 & 0 & 0 & 0 \\ 0 & 0 & 0 & -\Delta_3 & -\mu_d^g - M_d & k & 0 & 0 & 0 & 0 & 0 & 0 & -\Delta_1 \\ 0 & 0 & \Delta_3 & 0 & 0 & k & -\mu_d^g + M_d & 0 & 0 & 0 & 0 & \Delta_1 & 0 \\ 0 & \Delta_3 & 0 & 0 & 0 & 0 & \mu_d^g - M_d & k & 0 & 0 & \Delta_1 & 0 & 0 \\ -\Delta_3 & 0 & 0 & 0 & 0 & 0 & k & \mu_d^g + M_d & -\Delta_1 & 0 & 0 & 0 & 0 \\ 0 & 0 & 0 & -\Delta_2 & 0 & 0 & 0 & -\Delta_1 & -\mu_s^b - M_s & k & 0 & 0 & 0 \\ 0 & 0 & \Delta_2 & 0 & 0 & 0 & 0 & \Delta_1 & 0 & k & -\mu_s^b + M_s & 0 & 0 \\ 0 & \Delta_2 & 0 & 0 & 0 & \Delta_1 & 0 & 0 & 0 & 0 & \mu_s^b - M_s & k & 0 \\ -\Delta_2 & 0 & 0 & 0 & -\Delta_1 & 0 & 0 & 0 & 0 & 0 & k & \mu_s^b + M_s & 0 \end{pmatrix}. \quad (\text{A5g})$$

The eigenvalues of  $\mathcal{M}_+^{(1)}$  and  $\mathcal{M}_+^{(2)}$  for  $gu - rd$  pair are derived as:

$$\epsilon_i^{(1)} = \text{sign}_1 \sqrt{\left( \frac{\mu_d^r + \mu_u^g}{2} \text{sign}_2 \sqrt{M^2 + k^2} \right)^2 + \Delta_3^2} - \frac{\mu_d^r - \mu_u^g}{2}, \quad (\text{A6})$$

and

$$\epsilon_i^{(2)} = \text{sign}_1 \sqrt{\left( \frac{\mu_d^r + \mu_u^g}{2} \text{sign}_2 \sqrt{M^2 + k^2} \right)^2 + \Delta_3^2} + \frac{\mu_d^r - \mu_u^g}{2}, \quad (\text{A7})$$

where two signs,  $(\text{sign}_1, \text{sign}_2)$  of four eigenvalues ( $i = 1 - 4$ ) for each matrix are  $(\pm, \pm)$  and  $(\pm, \mp)$ . Note that we have use the approximation that  $\bar{M} = (M_u + M_d)/2$ , where the correction on the eigenvalues is

$$\delta\epsilon = \pm e \left( \frac{x}{2e^2} - \frac{x^2}{8e^4} + \mathcal{O}\left(\frac{x}{e^2}\right)^3 \right), \quad (\text{A8})$$

$x = M_{u(d)}^2 - \bar{M}^2$  and  $e = \sqrt{k^2 + M^2}$ , with the plus sign for the antiparticle mode and the minus sign for the particle mode. Note the last term in Eq (A6) or (A7) denotes the half of difference of the quark chemical potential between  $u$  and  $d$ ,  $\pm(\mu_d - \mu_u)/2$ . In the evaluation of  $x$ ,  $M_d$  is for the case of plus sign of  $\mu_d - \mu_u$  in the last term in the formula of absolute value of the eigenvalue, while  $M_u$  is for the case of negative one. The formulae of eigenvalues for  $\mathcal{M}_+^{(3,4)}$  for  $ru - bs$  and  $\mathcal{M}_+^{(5,6)}$  for  $gs - bd$  are similar.

For the CFL phase ( $\mu > 457$  MeV), the approximations of  $\Delta_1 = \Delta_2$  and  $M_u = M_d$  are valid. 12 eigenvalues for  $\mathcal{M}_+^{(7)}$  are calculated with MATHEMATICA. 4 eigenvalues are for  $ru - gd$  pair, which have similar forms to Eqs (A6) and (A7), while the rest eight values are much more complex, which are not presented here.

for the CSL case, for each flavor, one has

$$\Phi^- = \Delta_f (\gamma_3 \lambda_2 + \gamma_1 \lambda_7 + \gamma_2 \lambda_5). \quad (\text{A9})$$

With the similar procedure, dispersion relations for  $S_f^{-1}$  can be derived. The flavor structure is trivial for CSL phase, and decoupled from the matrix. For each flavor,  $S_f^{-1}$  is a  $24 \times 24$  (color: 3, Dirac:  $4 \times 2$ ) matrix. The inverse propagator for flavor  $f$  is

$$S_f^{-1}(p) = \begin{pmatrix} \not{p} + \mu_f \gamma^0 - M_f & \hat{\Delta}_f \\ -\hat{\Delta}_f^\dagger & \not{p} - \mu_f \gamma^0 - M_f \end{pmatrix}. \quad (\text{A10})$$

$\mu_f$  is the chemical potential for the quark of flavor  $f$ . The six dispersions are [43]:

$$\begin{aligned} E_{f;1,2} &= \sqrt{\varepsilon_f^2 + \mu_f^2 + |\Delta_f|^2} \mp 2\sqrt{\mu_f^2 \varepsilon_f^2 + |\Delta_f|^2 k^2}, \\ E_{f;3,5}^2 &= (\varepsilon_f - \mu_f)^2 + c_{f;3,5}^{(1)} |\Delta_f|^2 + \dots, \\ E_{f;4,6}^2 &= (\varepsilon_f + \mu_f)^2 + c_{f;4,6}^{(1)} |\Delta_f|^2 + \dots, \end{aligned} \quad (\text{A11})$$

where

$$\begin{aligned} c_{f;3,5}^{(1)} &= \frac{1}{2} \left[ 5 - \frac{\vec{k}^2}{\varepsilon_f \mu_f} \pm \sqrt{\left( 1 - \frac{\vec{k}^2}{\varepsilon_f \mu_f} \right)^2 + 8 \frac{M_f^2}{\varepsilon_f^2}} \right], \\ c_{f;4,6}^{(1)} &= \frac{1}{2} \left[ 5 + \frac{\vec{k}^2}{\varepsilon_f \mu_f} \pm \sqrt{\left( 1 + \frac{\vec{k}^2}{\varepsilon_f \mu_f} \right)^2 + 8 \frac{M_f^2}{\varepsilon_f^2}} \right]. \end{aligned} \quad (\text{A12})$$

In the expansions for  $E_{f;3,4,5,6}$ , higher orders of  $\Delta_f$ , e.g.  $\Delta_f^4$  are neglected in the calculation.

- [3] E. Witten, *Phys. Rev. D* **30**, 272 (1984).
- [4] E. Farhi and R. L. Jaffe, *Phys. Rev. D* **30**, 2379 (1984).
- [5] C. Alcock, E. Farhi, and A. Olinto, *Astrophys. J.* **310**, 261 (1986).
- [6] B. C. Barrois, *Nucl. Phys. B* **129**, 390 (1977).
- [7] M. Alford, K. Rajagopal, and F. Wilczek, *Nucl. Phys. B* **537**, 443 (1999), [arXiv:hep-ph/9804403 \[hep-ph\]](#).
- [8] J. Bardeen, L. N. Cooper, and J. R. Schrieffer, *Phys. Rev.* **108**, 1175 (1957).
- [9] I. A. Shovkovy and L. C. R. Wijewardhana, *Phys. Lett. B* **470**, 189 (1999), [arXiv:hep-ph/9910225 \[hep-ph\]](#).
- [10] T. Schäfer, *Nuclear Physics B* **575**, 269 (2000), [arXiv:hep-ph/9909574 \[hep-ph\]](#).
- [11] K. Rajagopal and F. Wilczek, *Phys. Rev. Lett.* **86**, 3492 (2001), [arXiv:hep-ph/0012039 \[hep-ph\]](#).
- [12] M. Alford, C. Kouvaris, and K. Rajagopal, *Phys. Rev. Lett.* **92**, 222001 (2004), [arXiv:hep-ph/0311286 \[hep-ph\]](#).
- [13] M. Alford, C. Kouvaris, and K. Rajagopal, *Phys. Rev. D* **71**, 054009 (2005), [arXiv:hep-ph/0406137 \[hep-ph\]](#).
- [14] M. Buballa, *Phys. Rept.* **407**, 205 (2005), [arXiv:hep-ph/0402234 \[hep-ph\]](#).
- [15] D. Blaschke, S. Fredriksson, H. Grigorian, A. M. Öztaş, and F. Sandin, *Phys. Rev. D* **72**, 065020 (2005), [arXiv:hep-ph/0503194 \[hep-ph\]](#).
- [16] S. B. Rüster, V. Werth, M. Buballa, I. A. Shovkovy, and D. H. Rischke, *Phys. Rev. D* **72**, 034004 (2005), [arXiv:hep-ph/0503184 \[hep-ph\]](#).
- [17] A. Schmitt, *Phys. Rev. D* **71**, 054016 (2005), [arXiv:nucl-th/0412033 \[nucl-th\]](#).
- [18] P. Fulde and R. A. Ferrell, *Phys. Rev.* **135**, 550 (1964).
- [19] A. I. Larkin and Y. N. Ovchinnikov, *Soviet Journal of Experimental and Theoretical Physics* **28**, 1200 (1969).
- [20] M. Alford, J. Berges, and K. Rajagopal, *Nuclear Physics B* **571**, 269 (2000), [arXiv:hep-ph/9910254 \[hep-ph\]](#).
- [21] A. Schmitt, Q. Wang, and D. H. Rischke, *Phys. Rev. Lett.* **91**, 242301 (2003), [arXiv:nucl-th/0301090 \[nucl-th\]](#).
- [22] Y. Nambu and G. Jona-Lasinio, *Phys. Rev.* **122**, 345 (1961).
- [23] Y. Nambu and G. Jona-Lasinio, *Phys. Rev.* **124**, 246 (1961).
- [24] K. Kikkawa, *Prog. Theor. Phys.* **56**, 947 (1976).
- [25] P. Rehberg, S. P. Klevansky, and J. Hüfner, *Phys. Rev. C* **53**, 410 (1996), [arXiv:hep-ph/9506436 \[hep-ph\]](#).
- [26] D. N. Aguilera, *Astrophys. Space Sci.* **308**, 443 (2007), [arXiv:hep-ph/0608041 \[hep-ph\]](#).
- [27] W.-L. Yuan and A. Li, *Astrophys. J.* **966**, 3 (2024), [arXiv:2312.17102 \[nucl-th\]](#).
- [28] J. R. Oppenheimer and G. M. Volkoff, *Phys. Rev.* **55**, 374 (1939).
- [29] G. Baym, C. Pethick, and D. Pines, *Nature (London)* **224**, 673 (1969).
- [30] R. P. Huebener, *Phys. Rept.* **13**, 143 (1974).
- [31] R. P. Huebener, *Magnetic Flux Structures in Superconductors* (Springer Berlin, Heidelberg, 1979).
- [32] G. Baym, C. Pethick, and D. Pikes, *Nature (London)* **224**, 674 (1969).
- [33] K. Iida and G. Baym, *Phys. Rev. D* **66**, 014015 (2002), [arXiv:hep-ph/0204124 \[hep-ph\]](#).
- [34] H. Heiselberg and C. J. Pethick, *Phys. Rev. D* **48**, 2916 (1993).
- [35] B. Zhang, *The Physics of Gamma-Ray Bursts* (Cambridge University Press, 2018).
- [36] V. V. Usov, *Phys. Rev. Lett.* **87**, 021101 (2001), [arXiv:astro-ph/0106226 \[astro-ph\]](#).
- [37] R. Ouyed, Ø. Elgarøy, H. Dahle, and P. Keränen, *Astron. Astrophys.* **420**, 1025 (2004), [arXiv:astro-ph/0308166 \[astro-ph\]](#).
- [38] E. P. Mazets, R. L. Aptekar, T. L. Cline, D. D. Frederiks, J. O. Goldsten, S. V. Golenetskii, K. Hurley, A. von Kienlin, and V. D. Pal'shin, *Astrophys. J.* **680**, 545 (2008), [arXiv:0712.1502 \[astro-ph\]](#).
- [39] W. Wang, R. Luo, H. Yue, X. Chen, K. Lee, and R. Xu, *Astrophys. J.* **852**, 140 (2018), [arXiv:1710.00541 \[astro-ph.HE\]](#).
- [40] C. Dehman, D. Viganò, N. Rea, J. A. Pons, R. Perna, and A. Garcia-Garcia, *Astrophys. J. Lett.* **902**, L32 (2020), [arXiv:2010.00617 \[astro-ph.HE\]](#).
- [41] Y.-P. Yang and B. Zhang, *Astrophys. J.* **919**, 89 (2021), [arXiv:2104.01925 \[astro-ph.HE\]](#).
- [42] S. D. Ryder, K. W. Bannister, S. Bhandari, A. T. Deller, R. D. Ekers, M. Glowacki, A. C. Gordon, K. Gourdji, C. W. James, C. D. Kilpatrick, W. Lu, L. Marnoch, V. A. Moss, J. X. Prochaska, H. Qiu, E. M. Sadler, S. Simha, M. W. Sammons, D. R. Scott, N. Tejos, and R. M. Shannon, *Science* **382**, 294 (2023), [arXiv:2210.04680 \[astro-ph.HE\]](#).
- [43] D. N. Aguilera, D. Blaschke, M. Buballa, and V. L. Yudichev, *Phys. Rev. D* **72**, 034008 (2005), [arXiv:hep-ph/0503288 \[hep-ph\]](#).